

## Production of ultracold molecules with chirped nanosecond pulses: Evidence for coherent effects

J. L. Carini,<sup>1,\*</sup> J. A. Pechkis,<sup>1,\*†</sup> C. E. Rogers III,<sup>1</sup> P. L. Gould,<sup>1</sup> S. Kallush,<sup>2</sup> and R. Kosloff<sup>3</sup>

<sup>1</sup>*Department of Physics, University of Connecticut, Storrs, Connecticut 06269, USA*

<sup>2</sup>*Department of Physics and Optical Engineering, ORT Braude, P.O. Box 78, Karmiel, Israel*

<sup>3</sup>*Department of Physical Chemistry and the Fritz Haber Research Center for Molecular Dynamics, The Hebrew University, 91094, Jerusalem, Israel*

(Received 22 October 2012; published 2 January 2013)

We use frequency-chirped light on the nanosecond time scale to produce ultracold  $^{87}\text{Rb}_2$  molecules in the lowest triplet state via the process of photoassociation. Comparing to quantum simulations of the molecular formation, we conclude that coherent stimulated emission plays an important role and is primarily responsible for the significant difference observed between positive and negative chirps.

DOI: [10.1103/PhysRevA.87.011401](https://doi.org/10.1103/PhysRevA.87.011401)

PACS number(s): 32.80.Qk, 37.10.Mn, 34.50.Rk

Applying the concepts of coherent control to the manipulation of ultracold systems is a topic of considerable current interest. Coherent control [1,2] usually involves internal degrees of freedom, such as molecular vibration and rotation, while cooling and trapping techniques [3] deal with external degrees of freedom. The time scales are also quite different: Coherent control is typically done with ultrafast lasers, while motion at ultralow temperatures is very slow. A particularly noteworthy convergence of these two fields is the formation of ultracold molecules from ultracold atoms by the process of photoassociation [4] (PA). This free-bound transition is a simple binary reaction starting with a narrow range of continuum energies, so coherence can be expected to play an important role [5].

In recent years there have been many proposals for PA with shaped ultrafast pulses [5] to efficiently form ultracold molecules [6] for their many potential applications in quantum information, precision spectroscopy, ultracold chemistry, and quantum dipolar systems. So far, experimental progress towards coherently controlled PA has been limited to photodestruction of already existing ultracold molecules [7,8] and coherent transients in PA with femtosecond pulses [9,10]. In recent work, we have used frequency-chirped light on the nanosecond time scale to coherently control laser-induced inelastic collisions. Because our nanosecond pulses are well matched to the long-range motion of the colliding atoms, the collision rate depends on the chirp direction [11] and shape [12]. In the present work, we apply our chirped pulses to the more easily modeled process of PA and directly detect the resulting ground-state molecules. We find that the formation rate depends on chirp direction, in agreement with quantum simulations. These simulations reveal that despite the presence of spontaneous emission, a significant portion of this dependence arises from a coherent effect: stimulated emission into a specific high vibrational level.

In the experiment [11], we illuminate ultracold  $^{87}\text{Rb}$  atoms with nanosecond-scale pulses of frequency-chirped light,

forming  $^{87}\text{Rb}_2$  via PA. These excited molecules subsequently radiatively decay into high vibrational levels ( $v''$ ) of the  $a^3\Sigma_u^+$  metastable state, which are detected by resonantly enhanced multiphoton ionization (REMPI). The ultracold atoms are provided by a phase-stable magneto-optical trap (MOT) loaded by a slow atomic beam from a separate source MOT. The atomic temperature and peak density are  $\sim 150 \mu\text{K}$  and  $\sim 5 \times 10^{10} \text{cm}^{-3}$ , respectively.

The frequency-chirped light is produced by modulating the injection current of an external-cavity diode laser with a 5 MHz triangle wave, but with programmed adjustments to produce approximately linear positive and negative chirps with equal slopes during the pulse. Each chirp covers  $\sim 1$  GHz in 100 ns and is centered on the PA transition, a strong line located 7.79 GHz below the  $5S_{1/2}(F=2) \rightarrow 5P_{3/2}(F'=3)$  asymptote and determined to have  $0_g^-$  character [13]. To minimize amplitude modulation, the chirped light injection locks a separate 150 mW slave diode laser [14]. A sequence of 40 ns FWHM Gaussian pulses is generated by switching with an acousto-optical modulator. The timing selects the central regions of either the positive or negative chirps.

REMPI detection of the resulting  $\text{Rb}_2$  molecules is performed with 5 ns, 4 mJ pulses from a pulsed dye laser tuned to  $\lambda = 601.9$  nm and focused to  $\sim 3$  mm diameter at the MOT. Based on previous work [13,15], this light ionizes high- $v''$  levels of the  $a^3\Sigma_u^+$  state expected to be populated by PA to long-range excited states. The REMPI spectrum is similar to that from molecules produced by MOT light and is dominated by a broad feature at 601.9 nm. Individual high-lying  $v''$  levels are not resolved due to the  $0.2 \text{cm}^{-1}$  laser bandwidth. The resulting  $\text{Rb}_2^+$  ions are accelerated to a Channeltron detector and distinguished from  $\text{Rb}^+$  by time of flight. The timing of the experiment is as follows. A sequence of up to  $5 \times 10^4$  chirped (or unchirped) pulses, at a repetition rate  $f = 5$  MHz, is applied to the trapped atoms, and 25  $\mu\text{s}$  later, the REMPI pulse fires and the ions are detected. The entire cycle is repeated at 10 Hz. The MOT beams are extinguished for 50  $\mu\text{s}$  centered on the REMPI pulse to avoid ionization of excited atoms. We use a sequence of chirped PA pulses, so to obtain the molecular formation rate  $R$ , we must account for the loss of molecules during this PA window. There is photodestruction of a  $a^3\Sigma_u^+$  molecules by subsequent chirped pulses at a time-averaged

\*These authors contributed equally to this work.

†Currently with the Joint Quantum Institute, University of Maryland, College Park, Maryland 20742, USA.

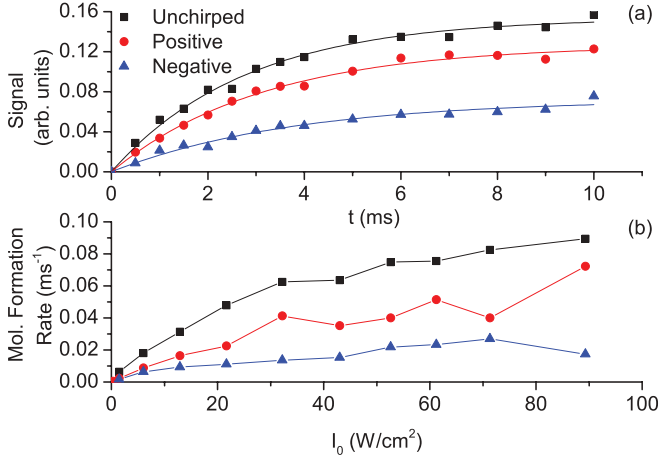


FIG. 1. (Color online) (a)  $\text{Rb}_2^+$  REMPI signals vs photoassociation time for unchirped, positively, and negatively chirped pulses, along with fits to Eq. (1). The peak intensity of the pulses is  $I_0 = 32.2 \text{ W/cm}^2$ . (b)  $\text{Rb}_2$  formation rate vs peak intensity for the various chirps.

rate  $\Gamma_{\text{PD}}$  as well as their escape from the detection region at a rate  $\Gamma_{\text{esc}}$ . The number  $N$  of detectable molecules evolves according to

$$N(t) = \frac{R}{\Gamma_{\text{PD}} + \Gamma_{\text{esc}}} (1 - e^{-(\Gamma_{\text{PD}} + \Gamma_{\text{esc}})t}). \quad (1)$$

We measure  $\Gamma_{\text{esc}} = 108(7) \text{ s}^{-1}$  using decay of the REMPI signal from MOT-produced molecules (i.e., without chirped light) as the REMPI pulse is delayed within a fixed 7 ms window following extinction of the MOT. We determine  $\Gamma_{\text{PD}}$  and  $R$  by varying the length of the PA window (i.e., the number of chirped pulses) and fitting to Eq. (1) as shown in Fig. 1(a). Here  $\Gamma_{\text{PD}} \sim 200 \text{ s}^{-1}$  for the positive chirp, implying a photodestruction probability of  $\sim 4 \times 10^{-5}$  per pulse.  $\Gamma_{\text{PD}}$  is linear in intensity and depends somewhat on chirp direction.

The quantity of interest is the formation rate  $R$  shown in Fig. 1(b). For each chirp direction,  $R$  increases with intensity but exhibits some degree of saturation. The important point is the pronounced dependence on chirp: The positive chirp has a rate higher than the negative chirp, but lower than the unchirped case.

To model the ultracold collisional dynamics, we solve the time-dependent Schrödinger equation. The dressed-state Hamiltonian reads

$$\hat{H} = \begin{pmatrix} \hat{T} + \hat{V}_{gJ} & \hbar\Omega_0(t) & \hbar\Omega_1(t) \\ \hbar\Omega_0^*(t) & \hat{T} + \hat{V}_0 + \hbar\Delta & 0 \\ \hbar\Omega_1^*(t) & 0 & \hat{T} + \hat{V}_1 + \hbar\Delta \end{pmatrix}, \quad (2)$$

where  $\hat{T}$  is the kinetic energy operator and  $\hat{V}_j$  [ $j = g, 0, 1$  for the  $^3\Sigma_u^+$ ,  $0_g^-(P_{3/2})$  and  $1_g(P_{3/2})$  electronic states] are the internuclear potentials [16] with coefficients [17] adjusted for the proper scattering length [18,19]. The two excited states correspond to the assignment of Ref. [13].  $\Delta/2\pi = -7.79 \text{ GHz}$  is the central detuning of the light from the asymptote [ $5S_{1/2}(F=2) + 5P_{3/2}(F'=3)$ ]. The  $0_g^-$  detuning is shifted [13] to yield the correct experimental spacing of  $\sim 0.6 \text{ GHz}$  and to be centered on  $\nu' = 78$ . For partial waves

beyond  $s$ , we add a rotational barrier  $V_J = J(J+1)/2\mu R^2$  to the  $^3\Sigma_u^+$  potential. Here  $\mu$  is the reduced mass.

The time-dependent couplings between the  $^3\Sigma_u^+$  ( $g$ ) and excited ( $j = 0, 1$ ) states due to the chirped pulse are given by  $\hbar\Omega_j = \mu_{gj}\epsilon_0 e^{[-\frac{(t-t_{\text{center}})^2}{2\sigma^2} + i\tilde{\omega}(t)(t-t_{\text{center}})]}$ , where  $\mu_{gj}$  are the  $R$ -independent transition dipole moments,  $\epsilon_0$  is the peak electric field,  $\sigma = 17 \text{ ns}$ ,  $t_{\text{center}}$  is the center of the pulse, and  $\tilde{\omega}(t)$  are instantaneous frequency offsets from  $\Delta$  derived from smoothed interpolations of the heterodyne signals [20].

To enable efficient computation for nanosecond timescales, we use a basis of vibrational levels calculated on a time-independent mapped Fourier grid [21–23]. In this new basis, the Hamiltonian reads

$$\hat{H} = \begin{pmatrix} \hat{H}_g & \hbar\hat{\Omega}_0(t) & \hbar\hat{\Omega}_1(t) \\ \hbar\hat{\Omega}_0^*(t) & \hat{H}_{e0} & 0 \\ \hbar\hat{\Omega}_1^*(t) & 0 & \hat{H}_{e1} \end{pmatrix}, \quad (3)$$

where  $\hat{H}_j$  are the vibrational energies from the field-free diagonalization and the  $\hat{\Omega}_j$  now include the Franck-Condon factors (FCFs). Since our experimental bandwidths are small ( $< 1 \text{ GHz}$ ) and our intensities are low ( $< 90 \text{ W/cm}^2$ ), a limited bandwidth above or below the relevant asymptote is taken to represent each of the vibrational Hamiltonians:  $\sim 15 \text{ GHz}$  for  $0_g^-$  and  $1_g$  and  $278 \text{ GHz}$  ( $16 \text{ MHz}$ ) for the  $^3\Sigma_u^+$  bound (scattering) manifold. We have verified that this representation is sufficient by extending the basis sets and checking convergence. The initial single state is a box-normalized scattering state at  $E_0 = k_B T$ , where  $T = 150 \text{ } \mu\text{K}$  is the sample temperature.

Spontaneous decay is accounted for by adding multiple sink channels, weighted by their FCFs, corresponding to decay from each of the excited-state ( $0_g^-$  and  $1_g$ ) vibrational levels [24] into various vibrational levels or the continuum of a  $^3\Sigma_u^+$ . Although this model precludes the possibility of multiple incoherent excitations, almost all of the population that decays into detectable levels is far from resonance and would therefore not participate in subsequent dynamics.

The computation gives the production probability per pulse,  $P_{E_0,J}$ , for a given initial box-normalized state and partial wave  $J$ . Following Ref. [25], we find the number of molecules per pulse:

$$N_{\text{mol},J} = \frac{\pi^2 \hbar^3 N n P_{E_0,J}}{\mu^{3/2} \sqrt{E_0} \left. \frac{dE}{dn} \right|_{E_0}}, \quad (4)$$

where  $n$  is the atomic density,  $N$  is the atom number, and  $\left. \frac{dE}{dn} \right|_{E_0}$  is the density of energy states evaluated at  $E_0$ . To find the formation rate for each intensity,  $R_J(I)$ , we multiply by the chirp repetition rate  $f$ :  $R_J(I) = N_{\text{mol},J} * f$ . Next, we spatially average over the Gaussian density distribution in the trap (average  $1/e^2$  radius =  $156 \text{ } \mu\text{m}$ ) and the Gaussian intensity profile of the photoassociation laser (average  $1/e^2$  radius =  $119 \text{ } \mu\text{m}$ ). Following Ref. [25], we find the overall formation rate at peak intensity  $I_0$  by summing over all partial waves necessary for convergence:  $R(I_0) = \sum_{J=0}^5 (2J+1) R_J(I_0)$ .

In Fig. 2 we plot these simulated  $\text{Rb}_2$  formation rates versus peak intensity for various chirped pulses. The values shown are derived from the total number of molecules in a  $^3\Sigma_u^+$

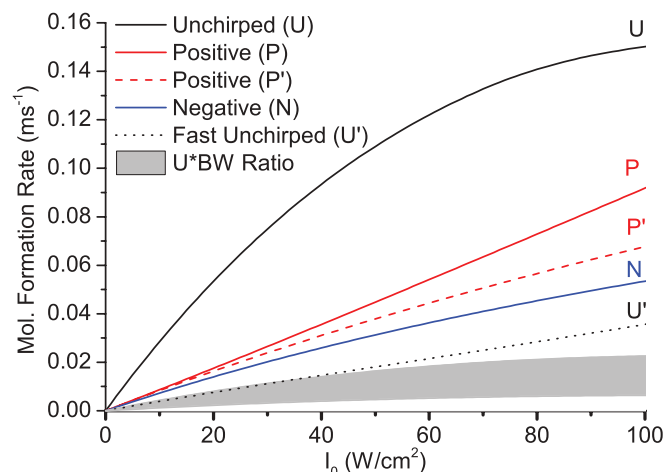


FIG. 2. (Color online) Simulated molecular formation rates vs peak intensity for unchirped (U), positively (P), and negatively (N) chirped pulses. The dashed curve (P') is for the positive chirp, but excluding the coherent contribution to  $v'' = 39$ . The shaded region is the range of results for the unchirped pulses scaled by the ratio of the unchirped bandwidth to the chirped bandwidth (see text). The dotted curve U' is for a pulse shorter by a factor of 48.

( $v'' = 0-39$ ) at  $t = 200$  ns after the beginning of the chirp. More than 93% of those molecules reside in  $v'' = 37-39$  and are thus within the REMPI bandwidth. The highest level,  $v'' = 40$ , is excluded because it is bound by only 39 MHz and therefore easily photodissociated by the chirped light. Also, its large outer turning point inhibits detection at our REMPI wavelength. The duration of the chirp is only 100 ns, but we allow spontaneous emission to run its course. Comparing to the experimental results in Fig. 1(b), we see good overall agreement, especially for the dependence on chirp: The rate for positive chirps exceeds that for negative chirps but is less than that for unchirped pulses.

Comparing chirped and unchirped results is problematic because the pulses have different bandwidths. Ultrafast pulse shaping in the frequency domain [26] leaves the frequency bandwidth fixed while stretching the pulse in time. In contrast, our addition of chirp in the time domain maintains the 40 ns FWHM pulse, but increases the bandwidth (FWHM) from the transform limit of 11 to 524 MHz. In the simulations, we vary the center detuning of the unchirped pulse, with the peak intensity fixed at 89.3 W/cm<sup>2</sup>, and find a 22 MHz FWHM when plotting formation rate versus detuning. Doing the same in the experiment, we find a bandwidth of 79 MHz. The limits of the shaded region of Fig. 2 indicate scalings of the unchirped results (curve U) by the ratio of each of these bandwidths to the chirped bandwidth of 524 MHz. This scaling allows a comparison at the same intensity per unit bandwidth. From this point of view, both the negative and positive chirps are more efficient than unchirped pulses. For completeness, we have also used a much shorter 0.84 ns FWHM unchirped pulse, increasing the peak intensity to keep the pulse energy fixed. This transform limit is 524 MHz, the same as for the 40 ns chirped pulses, but its simulated molecular formation rate (curve U' in Fig. 2) is lower. This is again consistent with higher efficiency for chirped PA at a fixed intensity per unit bandwidth.

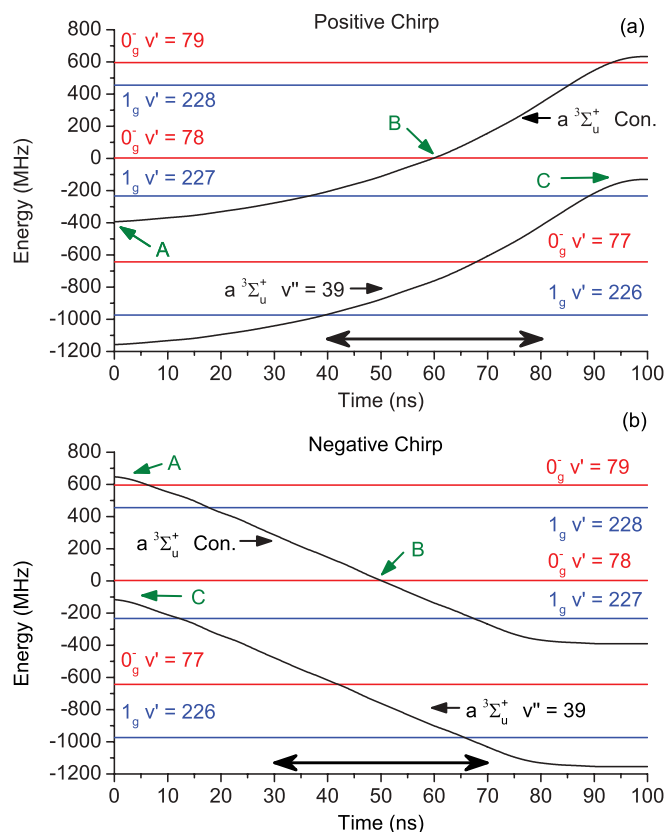


FIG. 3. (Color online) Evolution of the molecular levels during the positive (a) and negative (b) chirps. Horizontal lines are the relative energies of the vibrational levels of the excited  $0_g^-$  and  $1_g^-$  molecular states, while the energies of the  $a^3\Sigma_u^+$  zero-energy continuum and  $v'' = 39$  level, with the energy of the chirped photon added, are represented by the upper and lower black curves, respectively. In this picture, a curve crossing indicates resonance with the corresponding transition. Ground-excited couplings are not included in these plots. Double-ended arrows indicate the pulse widths (FWHM). The point labeled A is the initial continuum state, B indicates resonance with the  $0_g^-$  ( $v' = 78$ ) level, and C indicates the approach to resonance with the transition  $0_g^-$  ( $v' = 78$ )  $\rightarrow$   $a^3\Sigma_u^+$  ( $v'' = 39$ ).

The main conclusion from Figs. 1(b) and 2 is that the positive chirp gives a higher production rate than the negative chirp. By examining the evolutions of the various populations, we have identified the mechanism responsible for this difference. In Fig. 3, we show the relative energies of the excited levels involved in the chirp. We also show the  $a^3\Sigma_u^+$  zero-energy continuum and  $v'' = 39$  level, with the photon energy added. For clarity, the  $v'' = 40$  level, bound by only 39 MHz, is not shown. These time-dependent energies reflect the frequency variations of the chirps: positive in (a) and negative in (b). Curve crossings represent resonances with transitions between the corresponding states. For example, at point B in Fig. 3(a), the chirp is resonant with the PA transition from the zero-energy continuum to  $0_g^-$  ( $v' = 78$ ).

In Fig. 4, we plot the time-dependent populations of various excited and  $a^3\Sigma_u^+$  states. Figures 4(a) and 4(b) show the populations of the two dominant excited states,  $0_g^-$  ( $v' = 78$ ) and  $1_g^-$  ( $v' = 227$ ), respectively. As expected, the time ordering of population transfer to these states reverses with chirp

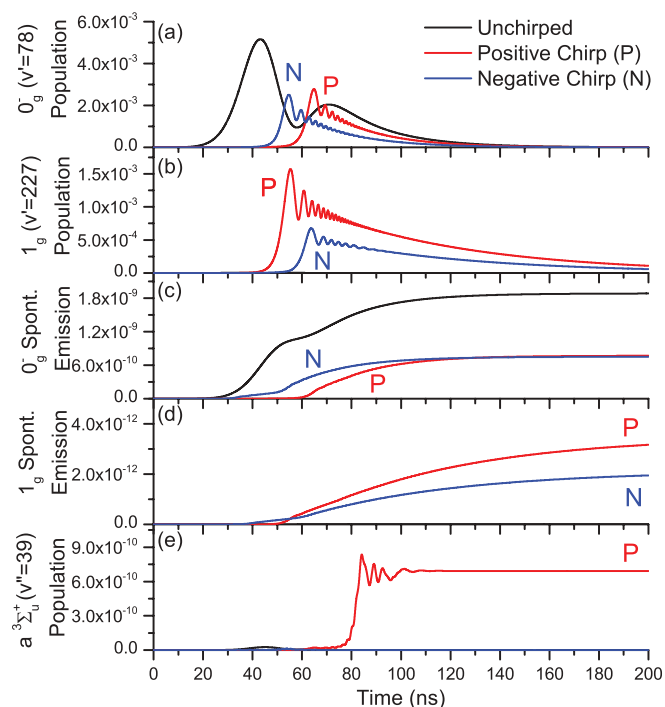


FIG. 4. (Color online) Populations of various molecular states during the unchirped, positively, and negatively chirped pulses for  $I_0 = 89.3 \text{ W/cm}^2$ : (a)  $0_g^- (v' = 78)$ , (b)  $1_g (v' = 227)$ , (c) a  $^3\Sigma_u^+$  bound levels populated by spontaneous emission (SE) from  $0_g^-$ , (d) a  $^3\Sigma_u^+$  bound levels populated by SE from  $1_g$ , (e) a  $^3\Sigma_u^+$  ( $v'' = 39$ ) resulting from stimulated emission from  $0_g^- (v' = 78)$ . Note that in (e), only the positive chirp has a significant contribution.

direction. The unchirped pulse excites only to  $0_g^- (v' = 78)$  since it is never resonant with  $1_g (v' = 227)$ . The excited-state populations eventually decay due to spontaneous emission. As shown in Figs. 4(c) and 4(d), a small fraction of these decays populates a  $^3\Sigma_u^+$  high- $v''$  levels, with  $0_g^-$  dominating due to better FCFs. Interestingly, as shown in Fig. 4(e), there is another contribution to  $v'' = 39$ , but only for the positive chirp. Referring back to Fig. 3(a), we see that at point C, resonance

between  $0_g^- (v' = 78)$  and  $^3\Sigma_u^+ (v'' = 39)$  is approached, and  $0_g^- (v' = 78)$  population is stimulated *down* to a  $^3\Sigma_u^+ (v'' = 39)$ . In contrast, for the negative chirp [Fig. 3(b)], C occurs near the beginning of the chirp, when there is no excited population to be stimulated down. The time ordering of these resonances is crucial to the population transfer and breaks the symmetry between positive and negative chirps. If we omit this coherent contribution to the formation rate for the positive chirp, we obtain curve P' in Fig. 2, demonstrating that this contribution is responsible for the majority of the difference between positive and negative chirps. The remaining difference is due to the shape variation between positive and negative chirps (Fig. 3). We have verified in the simulations that symmetric linear positive and negative chirps give identical results when this coherent contribution is omitted. This coherent contribution would be even larger if spontaneous emission did not deplete the excited-state population before the stimulated emission occurs.

In summary, we have investigated the formation of ultracold molecules using frequency-chirped light on the nanosecond timescale. We see a significant enhancement for the positive chirp relative to the negative chirp in both the experimental data and the quantum simulations. The evolutions of the various state populations reveal the mechanism responsible: photoassociation followed by stimulated emission into a high-vibrational level of a  $^3\Sigma_u^+$ . Although we observed a similar trend ( $\beta_{\text{pos}} > \beta_{\text{neg}}$ ) in the rate constant  $\beta$  for trap-loss collisions induced by chirped light [11,12,20], the mechanism here is quite different. The collisional work utilized smaller detunings and thus longer-range excitation, so the time scale of the chirp and the atomic motion were better matched. In the present work, the excited-state vibrational period is  $\sim 1.7 \text{ ns}$ , much shorter than the chirped pulses. Going to faster time scales and higher intensities, together with controlling the details of the chirped pulses [27], should allow further optimization of the molecular formation.

The work at the University of Connecticut is supported by the Chemical Sciences, Geosciences, and Biosciences Division, Office of Basic Energy Sciences, US Department of Energy.

- [1] S. A. Rice and M. Zhao, in *Optimal Control of Molecular Dynamics* (Wiley, New York, 2000).
- [2] M. Shapiro and P. Brumer, in *Principles of Quantum Control of Molecular Processes* (Wiley, New York, 2003).
- [3] H. J. Metcalf and P. van der Straten, in *Laser Cooling and Trapping* (Springer, New York, 1999).
- [4] K. M. Jones, E. Tiesinga, P. D. Lett, and P. S. Julienne, *Rev. Mod. Phys.* **78**, 483 (2006).
- [5] C. P. Koch and M. Shapiro, *Chem. Rev.* **112**, 4928 (2012), and references therein.
- [6] R. V. Krems, W. C. Stwalley, and B. Friedrich (eds.), *Cold Molecules: Theory, Experiment, Applications* (CRC Press, Boca Raton, FL, 2009).
- [7] W. Salzmann *et al.*, *Phys. Rev. A* **73**, 023414 (2006).
- [8] B. L. Brown, A. J. Dicks, and I. A. Walmsley, *Phys. Rev. Lett.* **96**, 173002 (2006).
- [9] W. Salzmann *et al.*, *Phys. Rev. Lett.* **100**, 233003 (2008).
- [10] D. J. McCabe, D. G. England, H. E. L. Martay, M. E. Friedman, J. Petrovic, E. Dimova, B. Chatel, and I. A. Walmsley, *Phys. Rev. A* **80**, 033404 (2009).
- [11] M. J. Wright, J. A. Pechkis, J. L. Carini, S. Kallush, R. Kosloff, and P. L. Gould, *Phys. Rev. A* **75**, 051401(R) (2007).
- [12] J. A. Pechkis, J. L. Carini, C. E. Rogers III, P. L. Gould, S. Kallush, and R. Kosloff, *Phys. Rev. A* **83**, 063403 (2011).
- [13] M. Kemmann, I. Mistrik, S. Nussmann, H. Helm, C. J. Williams, and P. S. Julienne, *Phys. Rev. A* **69**, 022715 (2004).
- [14] M. J. Wright, P. L. Gould, and S. D. Gensemer, *Rev. Sci. Instrum.* **75**, 4718 (2004).
- [15] C. Gabbanini, A. Fioretti, A. Lucchesini, S. Gozzini, and M. Mazzoni, *Phys. Rev. Lett.* **84**, 2814 (2000).

- [16] C. P. Koch and R. Kosloff, *Phys. Rev. A* **81**, 063426 (2010).
- [17] R. F. Gutterres, C. Amiot, A. Fioretti, C. Gabbanini, M. Mazzoni, and O. Dulieu, *Phys. Rev. A* **66**, 024502 (2002).
- [18] J. L. Roberts, N. R. Claussen, J. P. Burke Jr., C. H. Greene, E. A. Cornell, and C. E. Wieman, *Phys. Rev. Lett.* **81**, 5109 (1998).
- [19] S. Geltman and A. Bambini, *Phys. Rev. Lett.* **86**, 3276 (2001).
- [20] J. L. Carini, J. A. Pechkis, C. E. Rogers III, P. L. Gould, S. Kallush, and R. Kosloff, *Phys. Rev. A* **85**, 013424 (2012).
- [21] S. Kallush and R. Kosloff, *Chem. Phys. Lett.* **433**, 221 (2006).
- [22] S. Kallush, R. Kosloff, and F. Masnou-Seeuws, *Phys. Rev. A* **75**, 043404 (2007).
- [23] B. E. Londoño, A. Derevianko, J. E. Mahecha, A. Crubellier, and E. Luc-Koenig, *Phys. Rev. A* **85**, 033419 (2012).
- [24] P. S. Julienne and J. Vigué, *Phys. Rev. A* **44**, 4464 (1991).
- [25] C. P. Koch, R. Kosloff, E. Luc-Koenig, F. Masnou-Seeuws, and A. Crubellier, *J. Phys. B* **39**, S1017 (2006).
- [26] A. M. Weiner, *Rev. Sci. Instrum.* **71**, 1929 (2000).
- [27] C. E. Rogers III, M. J. Wright, J. L. Carini, J. A. Pechkis, and P. L. Gould, *J. Opt. Soc. Am. B* **24**, 1249 (2007).